

A Study on the Mathematical Modelling and Simulation of Large and Small Scale Structures in Star Formulation

Sumit Kumar Bajpeyee

Research Scholar M.Phil BRA University Muzaffarpur Bihar, India
M.Sc (Maths) M .S College Motihari

Abstract: *The aim of this paper is to show how a small scale and large scale star form. We also see some important factors which effect in star formulation. As for example these factors are gravity, temperature, velocity and magnetic field. In this paper generally I prefer magnetic property and The model assumes a prestellar core is threaded with a background magnetic field in the z-direction. Also The magnetic field governing protostellar cores plays an important role in star formation. The gas dynamics are influenced by the magnetic field, which regulates the gravity and can dictate the rate of formation. Polarimetry measurements provide the best tool for studying and inferring the magnetic properties. These limitations, theoretical models are commonly used in interpreting these measurements and inferring the respective observable properties*

Keywords: GPE, SFR, H2D+, MHD

1. Introduction

One of the foremost complicated processes in galaxies is star formation, and understanding it and its evolution with time remains a challenge for contemporary natural philosophy. The evolution of substance is currently modelled with high accuracy and is shaping the big scale structures within the universe. Stars square measure the foremost well known astronomical objects, and represent the foremost elementary building blocks of galaxies. The age, distribution, and composition of the celebs in a very galaxy trace the history, dynamics, and evolution of that galaxy. Moreover, stars square measure liable for the manufacture and distribution of significant parts like carbon, nitrogen, and oxygen, and their characteristics square measure intimately tied to the characteristics of the planetary systems that will coalesce concerning them. Consequently, the study of the birth, life, and death of stars is central to the sphere of ph 0079sics. Stars square measure born inside the clouds of mud and scattered throughout most galaxies. a well-known example of like a cloud is that the Orion Nebula. Turbulence deep inside these clouds offers rise to knots with comfortable mass that the gas and mud will begin to collapse underneath its own gravitational force. Because the cloud collapses, the fabric at the middle begins to heat up. referred to as a protostar, it's this hot core at the guts of the collapsing cloud that may sooner or later become a star. The subject of star formation is actually far more sophisticated than the preceding discussion suggests, part is inhabited with several sorts of clouds, fragments, protostars, stars, and nebulae. we are able to simply imagine increasing waves of matter driven outward by the high temperatures and pressures within the nebula. because the waves crash into the encircling molecular cloud, celestial body gas tends to compile and become compressed. The conclusion of cloud collapse may be a cluster of stars, all fashioned from a similar parent cloud and lying within the same region of space—in different words, a star cluster. As a by-product of cluster formation, a definite quantity of unused gas and mud remains.

2. Literature Survey

The physics of baryons, together with star formation, is far tougher to grasp and to implement in models of galaxy formation and evolution. Stars square measure born once pockets of gas and mud among heavenly body molecular clouds exceed essential density and collapse beneath their own gravity. Once the pressure and also the temperature within get high enough for nuclear reaction to ignite, it creates a star. The speed at that stars kind depends chiefly on the amount and density of those clumps among stellar nurseries. Scientists have currently used one feature of those clouds to raised perceive star formation, because the light-weight of distant stars penetrates through a stellar nursery, the molecular cloud's dirt dims the sunshine. By mensuration however this method dims thousands of various stars, scientists will reconstruct the cloud's 3D structure, serving to pinpoint however matter is distributed among the cloud. Some properties of star are - Distance can be determined from pure mathematics and qualitative analysis parallaxes. Also luminosity can be quantity of energy generated within the star and free as non particulate raditions. Brightness can not be a basic property while a mix level to and distance to star. These are the property of stars. Energy source of stars are - A really good question is how to star produce all that luminous energy, The answer should also naturally explain the main- sequence and the mass luminosity relation. Star produce some energy which radiates away into space. This answer explain that existence of the main sequence in the H-R diagram it leads to orbit make forward to the formation of new star or evolution stars.

Star forming region - Stars area unit born inside the clouds of mud/dust and scattered throughout most galaxies. a well-known example of like a cloud is that the Orion Nebula. Turbulence deep inside these clouds offers rise to knots with adequate mass that the gas and mud will begin to collapse beneath its own gravitation. Gravitation also plays an Important role in star formulation. The source of power for

Volume 12 Issue 3, March 2023

www.ijsr.net

[Licensed Under Creative Commons Attribution CC BY](https://creativecommons.org/licenses/by/4.0/)

star - forming is implosion, which should produce enough heat to ignite chemical element fusion in the protostar's gas at a temperature of about 15 million Kelvins. It's crucial to understand that the Jean's Mass is what must occur before a star may collapse. In the absent of other forces, gravity pulls things towards one another. Compared to the opposing forces, gravity is much weaker. When acting across scales bigger than the plan, it is occasionally the only one of the four. The mass of a star determines how long it will last. While small stars live longer lifetimes and eventually become white dwarfs, massive stars have brief lives that terminate in stellar explosions. Understanding a star's mass aids the United States in understanding not just the lifespan of a star but also the formation of galaxies. However precise, a star's mass is frequently problematic. Similarly velocity plays an Important role in star formulation.

Problem Definition

Here we are defining a mathematical model for simulation in large scale and small scale star formulation. Numerous characteristics of pre-stellar cores are related to the physical characteristics of the surrounding molecular cloud prior to changing collapse. A critical deterministic consideration for the soundness of a cloud is the threading force field. If the contraction process is gravitationally dominated, pulling field lines in the direction of contraction, the cloud is said to be magnetically supercritical.

Large scale and small scale structure in star formulation

The subcritical situation persists over considerably longer time frames (so called ambipolar diffusion time scales). The gradual movement of neutral particles towards the centre of the cloud will strengthen the quantitative relationship between mass and flux, or M/ϕ . In circumstances when the gravitational & magnetic contributions on contraction are exactly balanced, the critical ratio $(M/\phi)_{crit}$ is provided, and a cloud that's also magnetically subcritical does have a mass to flux ratio lower than that value. This is provided for situations when the gravitational & magnetic contributions

on contraction are exactly balanced. Once $M/\phi > (M/\phi)_{crit}$ Nowadays, the cloud has changed to a critical stage that heralds the beginning of self-propelled collapse. Unless there is internal thermal & turbulent pressure for support, a cloud that is initially in the critical condition experiences dynamical collapse sooner.

Mathematical model used in small scale structure star formulation.

The model, which is constructed using electromagnetism's fundamental equations, works best when used to match polarisation data. I employ the magnetic hourglass field model.

Model Descriptions

The model takes for granted that a prestellar core be threaded in the z-direction by a background magnetic field. Within the core, this backdrop field will be warped. Let B_0 denote the background field given as:

$$B_0 = B_0 \hat{z}$$

and so: The following is a formula for the total magnetic field :

$$B = B_c + B_0 \dots\dots\dots (1.1)$$

where B_c denotes the magnetic field produced locally inside the core. The model assumes that the magnetic field is axisymmetric about the ϕ -direction and the magnetic field is taken as $B \equiv B(r, z)$. The underlying premise of the assumption is that the model adequately captures the core and that the twists & irregularities in B_ϕ become significant only at the core's centre on a scale considerably smaller than the core's actual size. The magnetic field function of the model is directly derived from Maxwell's equations, and it produces an explicit analytical expression for such magnetic field components in the r and z directions for just a current density which is normally distributed all along vertical.

Hence, the magnetic vector potential has the following function:

$$A(r,z) = \sum_{m=1}^{\infty} k_m J_1(\sqrt{\lambda_m} r) \left[\operatorname{erfc}\left(\frac{\sqrt{\lambda_m} h}{2} + \frac{z}{h}\right) e^{z\sqrt{\lambda_m}} + \operatorname{erfc}\left(\frac{\sqrt{\lambda_m} h}{2} - \frac{z}{h}\right) e^{-z\sqrt{\lambda_m}} \dots\dots\dots (1.2)$$

For the co-efficient

$$k_m = \frac{2h\pi^{3/2} e^{h^2\lambda_m/4}}{CR^2 \sqrt{\lambda_m} [J_2(\sqrt{\lambda_m} R)]^2} \times \int_0^R f(\xi) J_1(\sqrt{\lambda_m} \xi) \xi d\xi \dots\dots\dots (1.3)$$

The formulas produced by the relation $B = \nabla \times A$, which provides the magnetic field, are as follows:

$$B_r(r, z) = \sum_{m=1}^{\infty} k_m \sqrt{\lambda_m} J_1(\sqrt{\lambda_m} r) \left[\operatorname{erfc}\left(\frac{\sqrt{\lambda_m} h}{2} - \frac{z}{h}\right) e^{-z\sqrt{\lambda_m}} - \operatorname{erfc}\left(\frac{\sqrt{\lambda_m} h}{2} + \frac{z}{h}\right) e^{z\sqrt{\lambda_m}} \right] \dots\dots\dots (1.4)$$

$$B_z(r, z) = \sum_{m=1}^{\infty} k_m \sqrt{\lambda_m} J_0(\sqrt{\lambda_m} r) \left[\operatorname{erfc}\left(\frac{\sqrt{\lambda_m} h}{2} + \frac{z}{h}\right) e^{z\sqrt{\lambda_m}} + \operatorname{erfc}\left(\frac{\sqrt{\lambda_m} h}{2} - \frac{z}{h}\right) e^{-z\sqrt{\lambda_m}} \right] + B_0$$

When the free parameters k_m , h, R, and B_0 are used

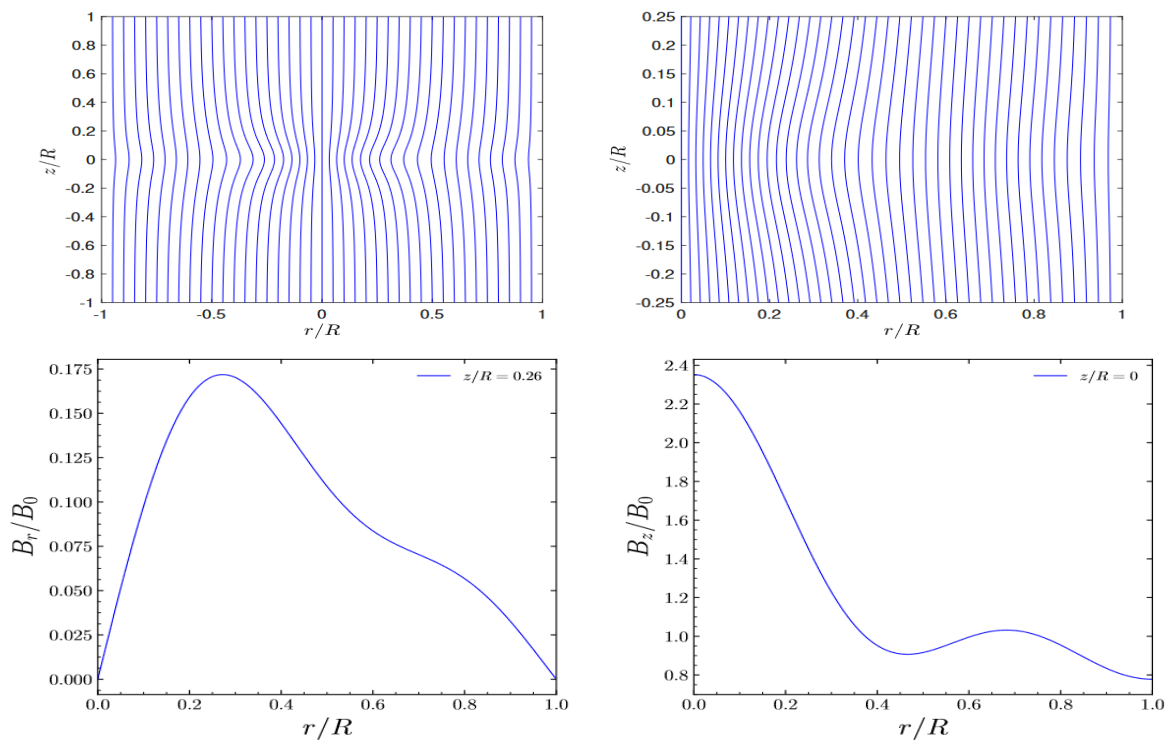


Figure 4: Magnetic field lines (top) and normalized field strength (bottom) using the parameters in the Basu and Ewertowski.

It is useful to talk about the model's fitting parameters, particularly for background field B_0 . According to Basu and Ewertowski (2013), the background field ought to be independent of the fit.

As it is exceedingly challenging to measure the magnetic field directly, one frequently uses indirect techniques that infer its magnetic field. Understanding how B_0 affects the

hourglass pattern can give insight as to what the B_0 should be in practice. The backdrop field will be changed and also the Basu, Ewertowski models would be utilised for demonstration purposes. The hourglass pattern is obscured and supplanted by B_0 even as background field intensity rises, as seen by the accompanying images. This is a common expectation, but the extra intriguing characteristic is what occurs so when field intensity is decreased.

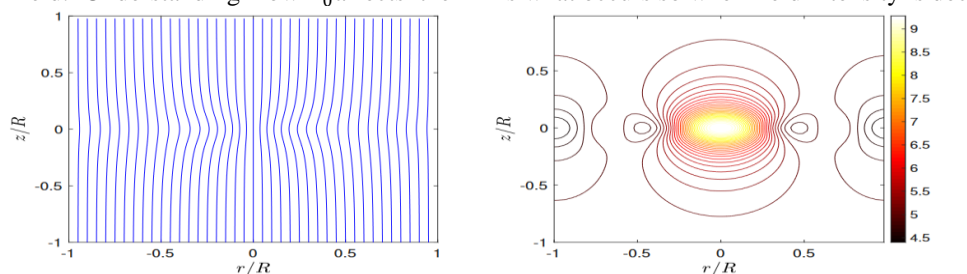


Figure 4: Background field $B = 0.5B_0$. Left: Magnetic field lines. Right: Contours of the total field strength.

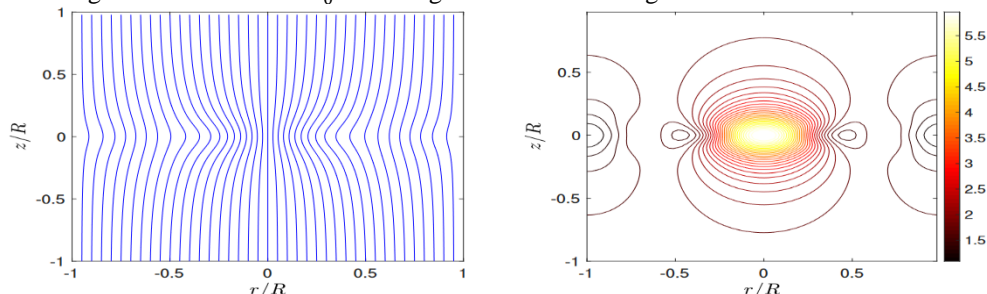


Figure 5: Background field $B = 0.25B_0$. Left: Magnetic field lines. Right: Contours of the total field strength.

The bulk of the sphere's strength is still concentrated in its centre, but as $B_0 \rightarrow 0$, the center's sandglass squeeze becomes more pronounced. The sphere lines between the core get more deformed as weaker that external field is.

This might provide information about how robust the background field is in relation to the core's sphere of

strength. Consequently, fitting a model that is normalised to a background field may make even more sense. One will rebuild 1.4 & 1.5 to being normalised to B_0 in order to provide solutions for B_r and B_z normalised to a background field because the background field may be difficult to live in directly. As polarisation maps only provide information for B_r/B_z , this may not change anything in terms to fitting

polarisation knowledge since, in principle, a normalised model will still be able to do so. Equations 1.4 & 1.5 must be scaled to a benchmark value in order to be normalised, and outputs must be expressed in terms of the same quantity.

Outline the following quantities adjusted to their respective benchmark variables once they are the same:

$$\tilde{r} = r/R \quad \tilde{z} = z/R \quad \eta = h/R \quad ; \quad \tilde{B}_r = B_r/B_0$$

$$\tilde{B}_z = B_z/B_0$$

Appendix A1.2 offers a dimensional analysis.

The amounts are entered into in the model equations for produce:

$$\tilde{B}_r \times B_0 = \sum_{m=1}^{\infty} k_m \sqrt{\lambda_m} J_1(\sqrt{\lambda_m} \tilde{r} R) \left[\operatorname{erfc} \left(\frac{\sqrt{\lambda_m} \eta R}{2} - \frac{\tilde{z} R}{\eta R} \right) e^{-\tilde{z} R \sqrt{\lambda_m}} - \operatorname{erfc} \left(\frac{\sqrt{\lambda_m} \eta R}{2} + \frac{\tilde{z} R}{\eta R} \right) e^{\tilde{z} R \sqrt{\lambda_m}} \right]$$

$$\tilde{B}_z \times B_0 = \sum_{m=1}^{\infty} k_m \sqrt{\lambda_m} J_0(\sqrt{\lambda_m} \tilde{r} R) \left[\operatorname{erfc} \left(\frac{\sqrt{\lambda_m} \eta R}{2} + \frac{\tilde{z} R}{\eta R} \right) e^{\tilde{z} R \sqrt{\lambda_m}} + \operatorname{erfc} \left(\frac{\sqrt{\lambda_m} \eta R}{2} - \frac{\tilde{z} R}{\eta R} \right) e^{-\tilde{z} R \sqrt{\lambda_m}} \right] + B_0$$

$$\tilde{B}_r = \sum_{m=1}^{\infty} \beta_m J_1(a_{m,1\tilde{r}}) \left[\operatorname{erfc} \left(\frac{a_{m,1\eta}}{2} - \frac{\tilde{z}}{\eta} \right) e^{-a_{m,1\tilde{z}}} - \operatorname{erfc} \left(\frac{a_{m,1\eta}}{2} + \frac{\tilde{z}}{\eta} \right) e^{a_{m,1\tilde{z}}} \right]$$

$$\tilde{B}_z = \sum_{m=1}^{\infty} \beta_m J_0(a_{m,1\tilde{r}}) \left[\operatorname{erfc} \left(\frac{a_{m,1\eta}}{2} + \frac{\tilde{z}}{\eta} \right) e^{a_{m,1\tilde{z}}} + \operatorname{erfc} \left(\frac{a_{m,1\eta}}{2} - \frac{\tilde{z}}{\eta} \right) e^{-a_{m,1\tilde{z}}} \right] + 1$$

where the dimensionless variable β_m has been defined to be:

$$\beta_m = \frac{k_m \sqrt{\lambda_m}}{B_0}$$

One should now request to fit the quantitative relation $B_r/B_z \equiv \tilde{B}_r/\tilde{B}_z$ to the relative angles established with the vertical axis when given polarisation information. The values for β_m remain the same, therefore the β_m terms advise that B_0 & R may be chosen at will. The numbers B_0 and R must scale in opposite directions in order to keep the model intact while still being relevant to the job.

Mathematical model used in small scale structure star formulation

Star formation is significantly influenced by the magnetic field regulating protostellar cores. The magnetic field affects gas dynamics because it controls gravity and can determine how quickly crystals form. The greatest instrument for analysing and extrapolating magnetic characteristics is provided by polarimetry data. Because to the scarcity of high-resolution polarisation data, inferring the magnetic field of protostellar cores can be difficult. Although though observationally measured polarisation maps have been few and challenging to get, some have recently been made public. In order to understand these observations and extrapolate the corresponding observable qualities, theoretical models are frequently employed due to these restrictions. Magnetohydrodynamic (MHD) simulation can be used to study the evolutionary characteristics regulating protostellar cores. Numerical MHD models has to be non-ideal so account for magnetic field's incomplete coupling to the plasma due to the clouds' weak ionisation. These simulation results serve as a basis for such a model that may be used to create synthetic polarisation maps by combining them with data from observed polarimetry. The magnetic fields at a particular orientation which is integrated along observer's line of sight is inferred using these synthetic maps. A sequence of protostellar models may be built at different length scales, solving smaller & smaller areas, by computationally solving all resistive MHD equations across a stacked grid. The radiative transfer algorithm POLARIS

may be used to replicate a specific polarisation map at a certain length scale for each model output. Inside a simulation cube with side lengths as tiny as $\approx 90 - 180$ au, these MHD simulations are utilised to create high resolution models. Predictions for upcoming higher resolution observations are made possible by these length scales, which can be smaller than a large portion of a observed polarimetry data now accessible.

Non-Ideal Magnetohydrodynamic Simulation

We develop a model based on non-ideal magnetohydrodynamic simulations to mimic the dense, star-forming centre of molecular clouds. This is frequently a natural progression from the preceding model. The clouds are mildly ionised in these thick areas, making it impossible for the magnetic field to couple to the plasma, invalidating the flux frozen property. In order to accommodate for neutrals, ions, electrons, and other charged particles, the plasma must now be handled in a very non-ideal MHD manner. Machida et al. used our 3-D nested MHD code to do the simulations, which solves all resistive MHD equations along with the self-gravity equations.

$$\frac{\partial \rho}{\partial t} + \nabla \cdot (\rho v) = 0 \dots \dots \dots (1.1)$$

$$\rho \frac{\partial v}{\partial t} + \rho(v \cdot \nabla)v = -\nabla p + j \times B - \rho \nabla \Phi \dots \dots \dots 1.2$$

$$\frac{\partial B}{\partial t} = \nabla \times (v \times B) + \eta \nabla^2 B \dots \dots \dots 1.3$$

$$\nabla^2 \phi = 4\pi G \rho \dots \dots \dots 1.4$$

for the magnetic field B , the velocity v , and the density ρ . Here, Φ is the gravitational potential, j is the electric current density, p is the pressure, η is the resistivity and G is the gravitational constant.

Initial State

Its core has the Bonnor-Ebert density profile in its initial condition, with a central density of $6 \times 10^5 \text{ cm}^{-3}$ and an isothermal temperature of $T = 10$ K.

$M_{cl} = 2M_{\odot}$ and $R_{cl} = 1.2 \times 10^4 au$ are assumed to represent the original core mass and radius, respectively.

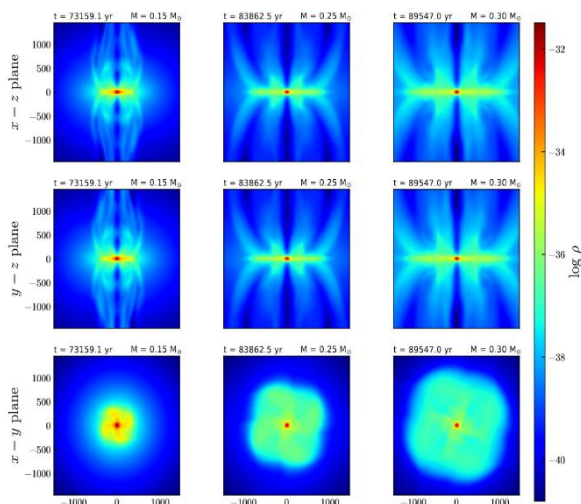
In order to facilitate the contraction, the simulation additionally increases cloud density by the factor of $f = 1.68$. For the starting core, a stiff rotation of $\Omega_0 = 1.3 \times 10^{-13} s^{-1}$ with an axis parallel to a magnetic field is taken, along with a constant magnetic fields of $B_0 = 3.2 \times 10^{-5} G$. Moreover, it is assumed that the starting state's normalised mass-to-flux ratio is $\mu_0 = 2$, which is normalised to a critical value $1/(2\pi G^{1/2})$. Last but not least, the proportions of thermal & rotational energy for gravitational energy are, respectively, $\alpha_0 = 0.42$ and $\beta = 0.024$.

MHD Simulation Output

The MHD simulations go up to $t \approx 89547$ years, or a mass of $M \approx 0.3M_{\odot}$ in the development of the core. At each level of the stacked grid, figures illustrate the simulation outcomes. As a result, each figure shows 8 or 9 distinct plots, ranging from level 5 through levels 12 and 13, inclusive.

The core's structure is examined in the simulations' principal analysis for three evolutionary stages: $M = 0.01M_{\odot}$, $M = 0.2M_{\odot}$ and $M = 0.28 M_{\odot}$. At all layers of the layered grid, those outputs will be expanded to simulate synthetic polarisation maps. High quality images of the tiny scale areas within protostellar cores will be possible because to this technology.

Figure 30 shows the temporal development of a plasma outflow even as core has developed to $M = 0.15M_{\odot}$, $M = 0.25M_{\odot}$ and $M = 0.30M_{\odot}$, in order to further help the viewer understand the dynamics of the core. These plots are exhibited in the x - z , y - z , and x - y planes or are taken on level 7 of the nested grid like a midplane cut just at 32nd cell.



Density (g/cm^3) is shown in Figure 4.2 to show how the outflow changes over time as the core changes. The level 7 stage of the simulation grid is depicted in the provided figure. The axis units specified are in au

Mass: $0.01 M_{\odot}$

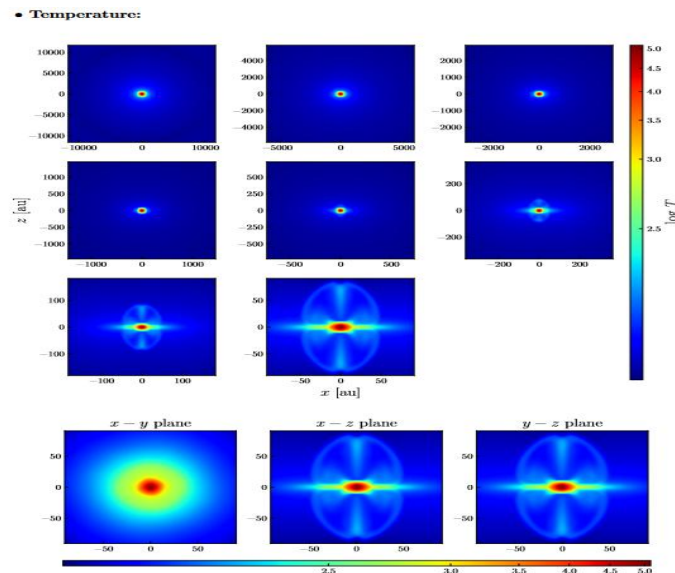


Figure 4.3: Top: Temperature (K) over all levels obtained at the 32nd cell of a slice across the y axis. Bottom: Level 12 temperature distribution at the 32nd cell for slices in the x , y , and z planes.

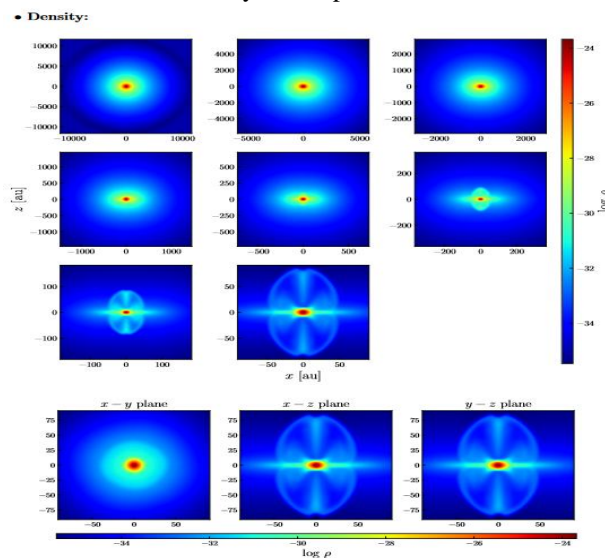
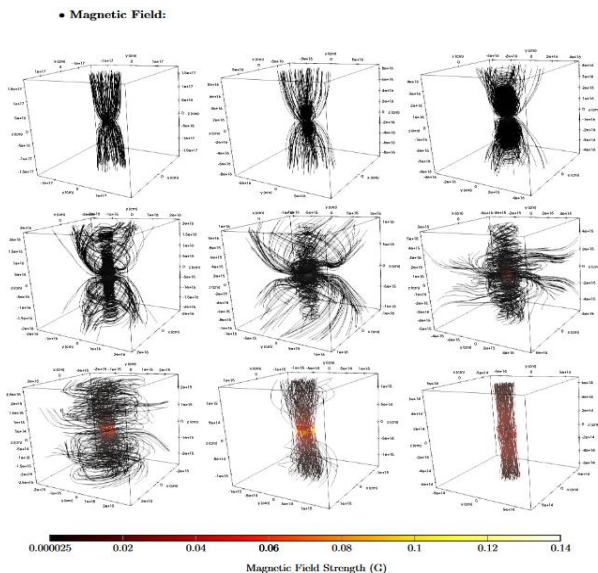


Figure 4.4: Top: Density (g/cm^3) for all levels as measured at the 32nd cell in a slice across the y plane. At the 32nd cell, slices across the x , y , and z plane show the density distribution of level 12 (bottom).



Three-dimensional magnetic field lines of levels 5 to 13 are shown in Figure 4.9. Levels 5, 6, and 7 at the top. Intermediate: Levels 8, 9, and 10. Levels 11, 12, and 13 at the bottom. The lower panels, which correspond to the upper levels, display the toroidal magnetic fields' growing effect at progressively smaller sizes.

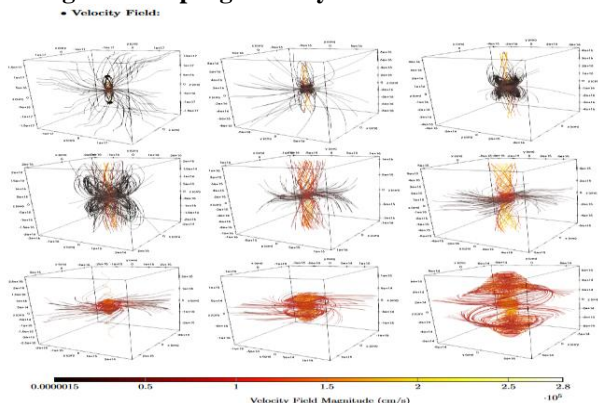


Figure 4.10.: Three dimensional velocity field lines for levels 5 - 13. Top: Levels 5, 6 and 7. Middle: Levels 8, 9 and 10. Bottom: Levels 11, 12 and 13

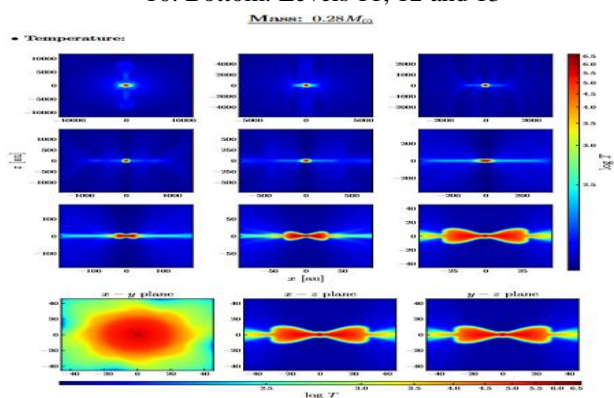


Figure 4.11: Top: Temperature (K) as all levels obtained at the 32nd cell of a slice across the y axis. Bottom: Level 13 temperature distribution at the 32nd cell for slices in the x, y, and z planes.

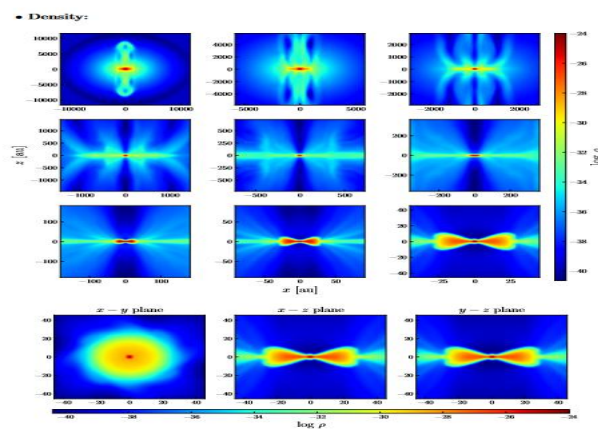
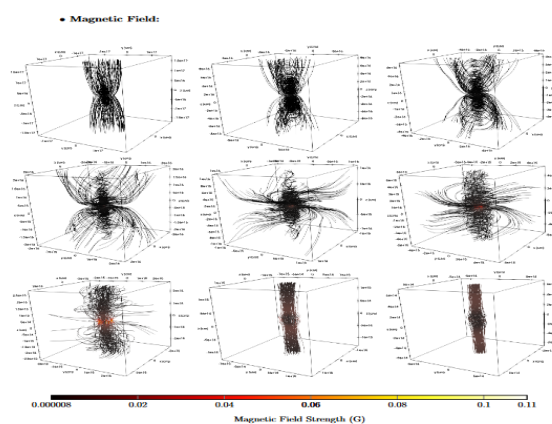
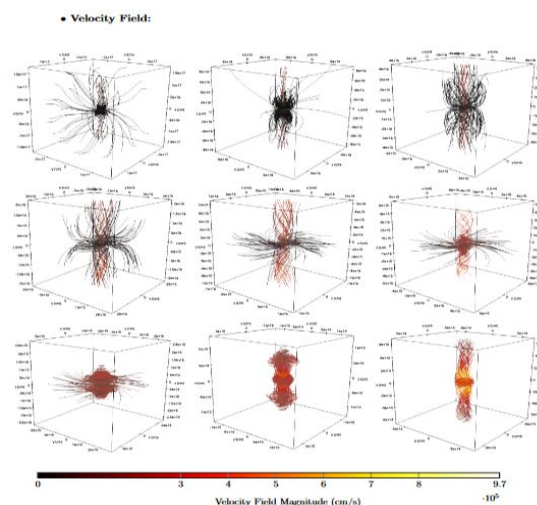


Figure 4.12: Top: Density (g/cm^3) for all levels as measured at the 32nd cell in a slice across the y plane. Distribution of density of level 13 for slices across the x, y, and z planes at the 32nd cell is shown at the bottom.



Three-dimensional magnetic field lines of levels 5 to 13 are shown in Figure 4.13.

Top: levels 5, 6, and 7. Bottom: Levels 11, 12, and 13. Middle: Levels 8, 9, and 10. The lower panels, which correspond to the upper levels, display the toroidal magnetic fields' growing effect at progressively smaller sizes.



Three-dimensional velocity field lines of levels 5 to 13 are shown in Figure 4.14. Levels 5, 6, and 7 at the top. Intermediate: Levels 8, 9, and 10. Levels 11, 12, and 13 at the bottom.

References

- [1] Bodifé, G., DeLoore, 1985. Oscillations in star formation and contents of a molecular cloud complex. *Astron Astrophys.* 142, 297.
- [2] Aalto, S., Hüttemeister, S., Scoville, N. Z., & Thaddeus, P. 1999, *ApJ*,
- [3] Adams, F. C., Hollenbach, D., Laughlin, G., & Gorti, U. 2004, *ApJ*, 611,
- [4] Adams, F. C., Lada, C. J., & Shu, F. H. 1987, *ApJ*, 312, 788
- [5] Afshordi, N., Mukhopadhyay, B., & Narayan, R. 2005, *ApJ*, 629, 373
- [6] Agertz, O., et al. 2006, *ArXiv Astrophysics e-prints*, arXiv:astro-ph/0610051
- [7] Alexander, R. D., Clarke, C. J., & Pringle, J. E. 2006a, *MNRAS*, 216
- [8] Allen, A., Li, Z.-Y., & Shu, F. H. 2003, *ApJ*, 599, 363.
- [9] Allen, A., Shu, F. H., & Li, Z.-Y. 2003, *ApJ*, 599, 351
- [10] Alves, J. F., Lada, C. J., & Lada, E. A. 2001, *Nature*, 409, 159
- [11] Anderson, J. M., Li, Z.-Y., Krasnopolsky, R., & Blandford, R. D. 2003, *ApJL*,
- [12] Andre, P., Belloche, A., Motte, F., & Peretto, N. 2006, *A & A*, in press Arce, H. G., & Sargent, A. I. 2006, *ApJ*, 646, 1070
- [13] Bacciotti, F., & Eislöffel, J. 1999, *A&A*, 342, 717
Balbus, S. A. 1988, *ApJ*, 324, 60
- [14] Walsh, W., Beck, R., Thuma, G., Weiss, A., Wiełebinski, R., & Dumke, M. 2002, *A&A*, 388, 7

Author Profile



Sumit Kumar Bajpeyee, M. Phil & Research Scholar,
BRA Bihar University, Muzaffarpur, Bihar.